

Impact analysis of the transponder time delay on radio-tracking observables

Stefano Bertone [1], Christophe Le Poncin-Lafitte [2], Pascal Rosenblatt [3], Valéry Lainey [4], Jean-Charles Marty [5], Marie-Christine Angonin [2]

[1] *Astronomical Institute, University of Bern, Switzerland*

[2] *SYRTE, Observatoire de Paris, PSL Research University, CNRS, Sorbonne Universités, UPMC Univ. Paris 06, LNE, 61 Avenue de l'Observatoire, 75014 Paris, France*

[3] *Royal Observatory of Belgium, Brussels, Belgium*

[4] *IMCCE, Observatoire de Paris, CNRS/UMR 8028, 61 Av. de l'Observatoire, F75014 Paris, France*

[5] *CNES/GRGS, OMP 14 avenue Édouard Belin 31400 Toulouse, France*

Abstract

Accurate tracking of probes is one of the key points of space exploration. Range and Doppler techniques are the most commonly used. In this paper we analyze the impact of the transponder delay, *i.e.* the processing time between reception and re-emission of a two-way tracking link at the satellite, on tracking observables and on spacecraft orbits. We show that this term, only partially accounted for in the standard formulation of computed space observables, can actually be relevant for future missions with high nominal tracking accuracies or for the re-processing of old missions. We present several applications of our formulation to Earth flybys, the NASA GRAIL and the ESA BepiColombo missions.

Keywords: space navigation, transponder delay, Doppler tracking, KBRR, orbit determination, light propagation

Email address: stefano.bertone@aiub.unibe.ch (Stefano Bertone [1])

1. Introduction

Accurate tracking of probes is one of the key points of space exploration. Several radio tracking strategies are possible to determine the trajectory of interplanetary spacecraft, but Doppler and Range techniques are the most commonly used. Precise orbits are then the basis of many scientific applications, from geodesy and geophysics to the study of planetary atmospheres, the correct interpretation of instrument data up to fundamental physics experiments.

Range accuracy improved by one order of magnitude during the last 10 years (from 1 meter for the NASA Cassini probe - [Hees et al. \(2014c\)](#) - to 10 cm for the ESA BepiColombo mission - [Milani et al. \(2001\)](#); [Genova et al. \(2012\)](#)) while, thanks to the development of X- and Ka-band transponders, Doppler accuracy increased drastically from ≈ 10 mHz for Pioneer Venus Orbiter (≈ 1.5 mm/s @ 2.2 GHz, [Konopliv et al., 1993](#)) to the μ Hz level for BepiColombo and for Juno (≈ 35 nm/s @ 8.4 GHz, [Galanti et al., 2017](#)). Improvements in the technical accuracy of these observables result in better constraints on their scientific interpretation and have consequences in several domains. For this reason, a continuous effort is necessary to keep up the modeling with the increasing accuracy of instruments and mission goals.

In both Range and Doppler techniques, tracking signals are exchanged between an antenna on Earth and the probe. The standard light-time formulation by [Moyer \(2003\)](#) accurately describes how to model this exchange and the resulting observables. However, the small time delay between the reception of the tracking signal on the probe and its re-emission back to Earth is currently neglected in the two-way Doppler formulation, while it is introduced as a simple calibration in the two-way range ([Montenbruck and Gill, 2000](#); [Moyer, 2003](#)). This time delay, which we call "transponder delay", represents the response time of the transponder electronics and it is around several μ s for modern transponders ([Busso \(TAS-I\), 2010](#)).

In this paper, we analyze the impact of including this term in the mathematical formulation of computed light-time and deep space Range and Doppler observables with the goal of improving the agreement between computed and observed quantities in the orbit determination process. Section 2 briefly summarizes the standard modeling as given by [Moyer \(2003\)](#). Then, in Section 3 we describe the introduction of the transponder delay in light-time modeling and in Section 4 its impact on the range and Doppler observables. Section 5 provides some examples of the impact of the additional terms in

several configurations such as an Earth swing-by, NASA GRAIL (Zuber et al., 2013) and ESA BepiColombo missions. Finally, in Section 6 we summarize our final remarks.

2. Standard modeling of light time for radioscience observables

The standard approach for space navigation is presented in Moyer (2003). It provides the formulation for observed and computed values of deep space navigation data. Only a cursory description is provided as required by the scope of this paper.

Orbit Data File (ODF) tracking data consist of time series of observed Range or Doppler counts. Both these observables can be computed as functions of the time of flight of the signal between the observing station and the probe, provided auxiliary information, *e.g.*, Doppler emitted frequency and count times, are available in the ODF. Moyer (2003) designates the transmission time from Earth of the up-leg link as t_1 , the epoch of reception and immediate re-transmission as t_2 and finally the reception time of the down-leg link on ground as t_3 . At each of these epochs the Solar System Barycentric (SSB) position vectors of the up-link station \mathbf{x}_1 , spacecraft \mathbf{x}_2 and down-link station \mathbf{x}_3 must be calculated.

All coordinates presented in this paper, unless differently stated, are defined in the Barycentric Reference System (BCRS, Petit and Luzum, 2010), while all epochs are consistently given in the Barycentric Dynamical Time (TDB, Petit and Luzum, 2010). Moreover, we shall neglect all transformations between coordinate and proper times, since the relative modification would be at most 10^{-8} , which is fully negligible.

Range observables are related to the distance between observer and receiver, while Doppler observables (in the Moyer's sense of instantaneous Doppler shifts averaged over a time interval T_c) provide a constraint on their relative radial velocity. These so called *computed observables* are then used in the orbit recovery process by means of a least square fit to the tracking observations .

2.1. Round-trip light time

The key point for the *computed observables* is to properly describe the round trip time of flight ρ of the light signal. The standard formulation by Moyer (2003) gives

$$\rho = \frac{R_{12}}{c} + \frac{R_{23}}{c} + RLT_{12} + RLT_{23} + \delta\rho \quad (1a)$$

where

$$\frac{R_{12}}{c} = t_2(ET) - t_1(ET) = \frac{\|\mathbf{x}_2 - \mathbf{x}_1\|}{c}, \quad (1b)$$

$$\frac{R_{23}}{c} = t_3(ET) - t_2(ET) = \frac{\|\mathbf{x}_3 - \mathbf{x}_2\|}{c}, \quad (1c)$$

and RLT_{ij} is the Shapiro delay (Shapiro, 1964) on the up-leg and down-leg light time solutions. Moreover, we noted $\delta\rho$ the additional delays (*e.g.*, atmospheric and instrumental delays at ground stations) and ET the ephemeris time. Since modern ephemeris also define the TDB consistently with planetary ephemeris (*e.g.*, Fienga et al., 2009; Folkner et al., 2014), from now on we set ET=TDB.

Also, one should correct the reception time for the distance between the antenna receiver and the station clock. For a spacecraft light-time solution, the reception time t_{3R} is usually given in Station Time (ST) at the receiving electronics. The transformation between ST (usually Coordinated Universal Time, UTC) and ET/TDB is provided in (Petit and Luzum, 2010). One should then correct for the down-leg delay at the receiver δt_3 to get the reception time $t_3(ST)$ at the tracking point of the receiver as

$$t_3 = t_{3R} - \delta t_3. \quad (2)$$

The same also applies to the emission time t_1 . Since one does not know the time of reception and re-transmission t_2 , the latter is usually determined by iteratively applying Eq. (1), *i.e.*, by first considering $t_2 \equiv t_3$ to compute ρ , then setting $t_2 \equiv t_3 - \rho$.

3. Improved light time modeling

The standard formulation presented in Section 2 implies an instantaneous retransmission of the signal towards Earth after reception at the spacecraft. In reality, a small delay due to the transponder electronics should be accounted for, which is not provided in the standard auxiliary data. We report in Table 1 this transponder delay for several probes, as calibrated by industrials on ground before the launch.

Let us note $\Delta\tau$ this delay in terms of local proper time at the moment and location of the calibration. In our modeling, we have introduced the transponder delay δt_{23} in the BCRS between reception and remission events

Spacecraft	Launch	TD	Source
MPO	2018	4.8-6	†
Herschel	2009	5.2	†
Planck	2009	5.2	†
MRO	2005	1.4149	JPL
Venus Express	2005	2.085	ESOC/FD
Messenger	2004	1.371	★
Rosetta	2004	4.8-6	†
Mars Express	2003	2.076	ESOC/FD
Mars Odissey	2001	1.4266	JPL
Cassini	1997	4.8-6	†
MGS	1996	0.7797	MGS Project

Table 1: Transponder Delay (TD, μs) for several probes (MPO = BepiColombo Mercury Planetary Orbiter, MRO = Mars Reconnaissance Orbiter, MGS = Mars Global Surveyor, † = Busso (TAS-I) (2010), ★ = Srinivasan et al. (2007)).

at the probe. In principle, we should relate the calibrated transponder delay $\Delta\tau$ with δt_{23} . However, the impact of this additional correction shall prove negligible for our purpose, so that in the following $\delta t_{23} \equiv \Delta\tau$.

3.1. Studied setup

To take into account the transponder delay in the formulation of the light time solution, we need one supplementary event concerning the probe. Let us now consider four events quoted as \tilde{t}_i . The transmission epoch from Earth is quoted \tilde{t}_1 , \tilde{t}_2 is the epoch when the probe received the up-link signal, \tilde{t}_3 is the epoch of transmission of the transponded signal towards the Earth and finally \tilde{t}_4 is the epoch of reception of the down-link signal at receiving Earth ground station. We consistently note as \mathbf{x}_i the corresponding position vectors of tracking stations and probe. The light-time solution is composed of three steps: first we have to determine from the knowledge of the reception event by the Earth receiver the coordinate quantity $\tilde{t}_4 - \tilde{t}_3$, then to calculate $\tilde{t}_2 - \tilde{t}_1$. The third component deals with the internal electronics delay on-board the probe $\tilde{t}_3 - \tilde{t}_2$, *i.e.* all kinds of delay between the up-link reception and the down-link emission.

Our final goal is to express the coordinate quantity $\tilde{\rho} = \tilde{t}_4 - \tilde{t}_1$ which is simply $\tilde{t}_4 - \tilde{t}_1 = (\tilde{t}_4 - \tilde{t}_3) + (\tilde{t}_3 - \tilde{t}_2) + (\tilde{t}_2 - \tilde{t}_1)$. Let us quote the coordinate-dependent quantity $\tilde{t}_3 - \tilde{t}_2$ by δt_{23} . The quantities $\tilde{t}_2 - \tilde{t}_1$ and $\tilde{t}_4 - \tilde{t}_3$ can be expressed as

$$\tilde{t}_2 - \tilde{t}_1 = \mathcal{T}_r(\tilde{t}_2, \mathbf{x}_1, \mathbf{x}_2) , \quad (3a)$$

and

$$\tilde{t}_4 - \tilde{t}_3 = \mathcal{T}_r(\tilde{t}_4, \mathbf{x}_4, \mathbf{x}_3) , \quad (3b)$$

where we used the time transfer functions \mathcal{T}_r introduced in previous publications (Teyssandier and Le Poncin-Lafitte, 2008; Hees et al., 2014b). These functions essentially represent the light travel time between two events in a relativistic framework and have an analytical solution at several levels of approximation (*e.g.*, up to the third post-Minkowskian approximation for a static space-time (Linnet and Teyssandier, 2013) and at the first post-Minkowskian/post-Newtonian approximation for a set of moving axisymmetric bodies (Bertone et al., 2014; Hees et al., 2014a)). Hence, at the post-Newtonian level of approximation usually adopted in space navigation for a stationary gravity field, one gets

$$\mathcal{T}_r(t_i, \mathbf{x}_i, \mathbf{x}_j) = \frac{R_{ij}}{c} + RLT_{ij} + \mathcal{O}[c^{-4}] . \quad (4)$$

It is then straightforward to define the modified round-trip light time $\tilde{\rho} \equiv \tilde{t}_4 - \tilde{t}_1 + \delta\rho$ as

$$\tilde{\rho} = \delta t_{23} + \mathcal{T}_r(\tilde{t}_2, \mathbf{x}_2, \mathbf{x}_1) + \mathcal{T}_r(\tilde{t}_4, \mathbf{x}_4, \mathbf{x}_3) + \delta\rho , \quad (5)$$

where we noted $\delta\rho$ the additional delays (*e.g.*, atmospheric and instrumental delays), supposed equivalent to those given in Eq. (1a).

3.2. Comparison to the standard formulation

As we have seen in Eq. (1a), the traditional approach used by navigators does not consider the transponder delay in the light time formulation. This results in rewriting Eq. (1a) as

$$\rho = \mathcal{T}_r(t_2, \mathbf{x}_2, \mathbf{x}_1) + \mathcal{T}_r(t_3, \mathbf{x}_3, \mathbf{x}_2) + \delta\rho , \quad (6)$$

consisting only in three events t_1 , t_2 and t_3 . A relation between the \tilde{t}_l events of our proposed setup and the t_l of the standard setup is easily established by

setting (similarly to what proposed in a different context by [Degnan, 2002](#))

$$\tilde{t}_4 = t_3, \quad (7a)$$

$$\tilde{t}_3 = t_2, \quad (7b)$$

$$\tilde{t}_2 = \tilde{t}_3 - \delta t_{23} = t_2 - \delta t_{23} \quad (7c)$$

and

$$\tilde{t}_1 = t_1 - \Delta\rho, \quad (7d)$$

where we used $\Delta\rho = \tilde{\rho} - \rho \equiv (\tilde{t}_4 - \tilde{t}_1) - (t_3 - t_1)$ as well as Eq. (7a). As a consequence, we also get

$$\mathbf{x}_2(\tilde{t}_2) = \mathbf{x}_2(t_2 - \delta t_{23}), \quad (8a)$$

$$\mathbf{x}_1(\tilde{t}_1) = \mathbf{x}_1(t_1 - \Delta\rho). \quad (8b)$$

Thus, it is straightforward to analyze the difference between Eq. (5) and Eq. (6). Since the transponder delay δt_{23} is roughly equal to several μs (see Table 1), we perform a Taylor expansion of Eq. (5) and we introduce Eqs.(7)-(8), such that

$$\begin{aligned} \tilde{\rho} &= \mathcal{T}_r(t_2 - \delta t_{23}, \mathbf{x}_2 - \mathbf{v}_2 \delta t_{23}, \mathbf{x}_1 - \mathbf{v}_1 \Delta\rho) + \delta t_{23} \\ &\quad + \mathcal{T}_r(t_3, \mathbf{x}_3, \mathbf{x}_2) + \delta\rho \\ &= \mathcal{T}_r(t_2, \mathbf{x}_2, \mathbf{x}_1) + \delta t_{23} + \mathcal{T}_r(t_3, \mathbf{x}_3, \mathbf{x}_2) + \delta\rho \\ &\quad - \delta t_{23} \left. \frac{\partial \mathcal{T}_r(t, \mathbf{x}_2, \mathbf{x}_1)}{\partial t} \right|_{t=t_2} \\ &\quad - \delta t_{23} v_2^i \left. \frac{\partial \mathcal{T}_r(t_2, \mathbf{x}, \mathbf{x}_1)}{\partial x^i} \right|_{\mathbf{x}=\mathbf{x}_2} \\ &\quad - \Delta\rho v_1^i \left. \frac{\partial \mathcal{T}_r(t_2, \mathbf{x}_2, \mathbf{x})}{\partial x^i} \right|_{\mathbf{x}=\mathbf{x}_1} + \mathcal{O}[(\delta t_{23}, \Delta\rho)^2] \\ &\equiv \rho - \delta t_{23} \left. \frac{\partial \mathcal{T}_r(t, \mathbf{x}_2, \mathbf{x}_1)}{\partial t} \right|_{t=t_2} \\ &\quad - \delta t_{23} v_2^i \left. \frac{\partial \mathcal{T}_r(t_2, \mathbf{x}, \mathbf{x}_1)}{\partial x^i} \right|_{\mathbf{x}=\mathbf{x}_2} \\ &\quad - \Delta\rho v_1^i \left. \frac{\partial \mathcal{T}_r(t_2, \mathbf{x}_2, \mathbf{x})}{\partial x^i} \right|_{\mathbf{x}=\mathbf{x}_1} + \mathcal{O}[(\delta t_{23}, \Delta\rho)^2], \end{aligned} \quad (9)$$

where $\mathbf{v}_l = \{v_l^i\}$ is the coordinate velocity of the probe at instant t_l . It is worth noting that since an analytical formulations of the time transfer

function \mathcal{T}_r is available at various level of approximation, Eq.(9) can be easily adapted for increasing accuracies. For this application it is sufficient to expand \mathcal{T}_r using Eq. (4), which finally gives

$$\Delta\rho = \tilde{\rho} - \rho = \delta t_{23} \left(1 + \frac{(\mathbf{v}_1 - \mathbf{v}_2) \cdot \mathbf{N}_{12}}{c} \right) + \mathcal{O} [(\delta t_{23})^2, c^{-2}] \quad (10)$$

with

$$\mathbf{N}_{12} \equiv \frac{\mathbf{x}_2 - \mathbf{x}_1}{\|\mathbf{x}_2 - \mathbf{x}_1\|}.$$

While the constant term δt_{23} is usually calibrated in the computed Range, Eq. (10) highlights the presence of an extra non-constant term, directly proportional to the transponder delay and neglected in Moyer's model. This term also depends on the position and velocity of both the probe and the ground station.

It can be physically interpreted as a modification of the determination of the state vector at transponding event of coordinate time t_2 or as an imprecise determination of the time t_2 . Both range and Doppler are then affected by this mismodeling, as we show in Section 4.

4. Impact on Range and Doppler computed observables

Based on the standard and modified formulation of the light time ρ and $\tilde{\rho}$, respectively, we derive additional terms appearing in Range and Doppler observables.

The computed Range Observable R is simply given by

$$R = K\rho, \quad (11)$$

where K is a conversion factor. Depending on the processing strategies, the transponder delay δt_{23} is either added to ρ or estimated together with other error sources in a so called "range bias". However, both these solutions do not fully account for the impact of the transponder delay as given by Eq. (10), in particular regarding the time dependent terms.

Regarding Doppler, the basic idea is to measure the frequency shift based on the emission and reception times of a series of signals over a given time interval. Several configurations are possible. Two and three-way Doppler (in the latter the signal is emitted and received by different stations) are usually ramped, meaning that the emitted frequency f_T changes with time following

a piecewise linear function of time. For our purpose, we consider a simple modeling of unramped two-way Doppler F_2 , such that $\frac{\partial f_T}{\partial t} = 0$. Hence,

$$F_2 = \frac{M_2 f_T}{T_c} (\rho_e - \rho_s), \quad (12)$$

where M_2 is a multiplying factor related to the transponded frequency and ρ_e and ρ_s are the light-times of two signals whose receptions are separated by a "counting time" T_c , typically of the order of 10 – 60 s.

The difference between computing a Doppler observable with the two formulations presented in this paper is then given by introducing Eq. (10) into Eq. (12) as

$$\begin{aligned} \Delta F_2 &= \tilde{F}_2 - F_2 \\ &= \frac{M_2 f_T}{T_c} [(\tilde{\rho}_e - \tilde{\rho}_s) - (\rho_e - \rho_s)] \\ &= \frac{M_2 f_T}{T_c} \frac{\delta t_{23}}{c} [(\mathbf{v}_1^e - \mathbf{v}_2^e) \cdot \mathbf{N}_{12}^e - (\mathbf{v}_1^s - \mathbf{v}_2^s) \cdot \mathbf{N}_{12}^s]. \end{aligned} \quad (13)$$

The transponder delay δt_{23} itself is simplified when differencing, but not its impact on the Doppler frequency. Indeed, the epochs at which both the spacecraft and ground station positions are evaluated in the uplink change.

5. Numerical applications

In this section we present some examples to analyze the impact of the transponder delay δt_{23} in some realistic configurations. First, we compute the time dependent terms given in Eqs. (10) and (13) during the Earth flyby of several probes. Then, we show how the transponder delay can be easily introduced in the processing pipeline of Doppler data by explicitly adding a constant δt_{23} to the light-time algorithm as in Eq. (7c), thus retrieving the probe trajectory at a (slightly) different epoch. We perform the latter test on the GRAIL and BepiColombo missions within the planetary extension of the Bernese GNSS Software (BSW, [Dach et al., 2015](#)), mainly based on [Moyer \(2003\)](#) for the computation of deep space observables ([Bertone et al., 2015](#)).

5.1. Application to Earth flybys

In order to evaluate the magnitude of the additional term in Eq. (10), we compute $\Delta \rho = \tilde{\rho} - \rho$ and its time derivative $\Delta \dot{\rho} = \dot{\tilde{\rho}} - \dot{\rho} = \frac{\Delta F_2}{M_2 f_T}$,

i.e., the difference between the range-rate calculated by the two models. We consider several probes (Rosetta, NEAR, Cassini, Galileo) during their Earth flyby, which is a particularly favorable configuration thanks to the quick changes in the relative velocity vector between probe and antenna. Also, close approaches are an important source of information when measuring the geophysical parameters of a celestial body. We use the NAIF/SPICE toolkit (Acton et al., 2011) to retrieve the ephemeris for probes and planets to be used in the computation.

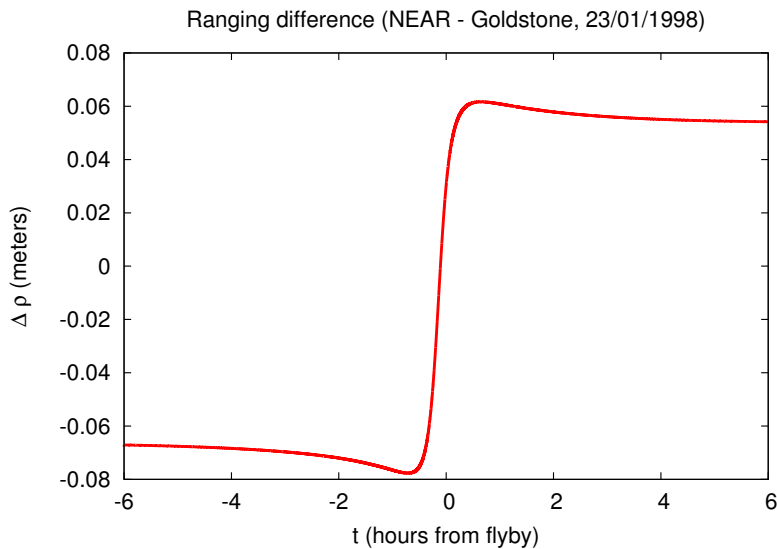


Figure 1: Light time difference $\Delta\rho$ (meters - hours from flyby) during NEAR Earth flyby.

We fix $\delta t_{23} = 10 \mu\text{s}$ and compute Eq. (10) and its time derivative from Eq. (13) for the NEAR probe during its Earth flyby on 23 January 1998. We find a difference of the order of some cm for the probe distance $c\Delta\rho$ calculated by the two models (when subtracting the constant δt_{23} bias) and a difference up to several $10^{-2} mm/s$ at the instant of maximum approach for its velocity. These results are shown in Figures 1 and 2 for $T_c = 1$ s. We note that changing the integration time T_c only has a significant impact when it becomes larger than several minutes. Also, results for other δt_{23} values can be easily deduced as $\Delta\rho$ and $\Delta\dot{\rho}$ are directly proportional to the transponder delay. The amplitude of such effects are in principle within the nominal accuracy of future missions expected to perform Earth gravity-assist maneuvers, such as BepiColombo.

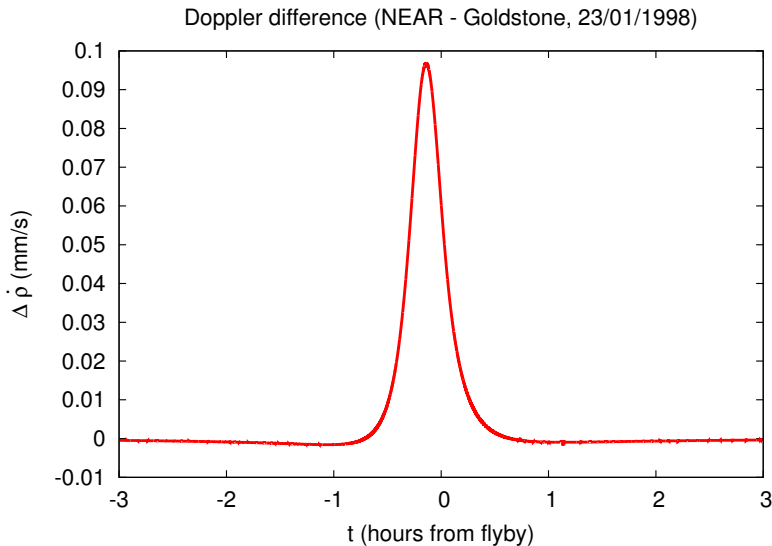


Figure 2: Range-rate difference $\Delta \dot{\rho}$ (mm/s - hours from flyby) during NEAR Earth flyby.

In order to highlight the high variability of the transponder delay effect on Doppler measurements, we also compute $\Delta \dot{\rho}$ for different probes in different configurations with respect to the observing station. The results displayed in Figure 3 show that this delay cannot be simply calibrated by adding a constant Range bias and hint that it should be carefully dealt with for the Doppler computation.

A preliminary study presented in Bertone et al. (2013) compared the results of this section with the so called flyby anomaly (Anderson et al., 2008) but found the mismodeling of the transponder delay to possibly account only for a few percent of it.

5.2. Application to GRAIL Doppler and KBRR data

Here, we use the BSW to process two-way S-band Doppler data and to retrieve GRAIL-A and GRAIL-B orbits around the Moon for several days of the primary mission phase. In particular, we selected both days when the orbital plane was parallel (days 63-64 of year 2012) and when it was perpendicular (days 72-73 of year 2012) w.r.t. the line of sight between the satellites and the Earth. We fit a set of 6 orbital elements in daily arcs using GRGM900C (Lemoine et al., 2014) up to d/o 600 as background gravity

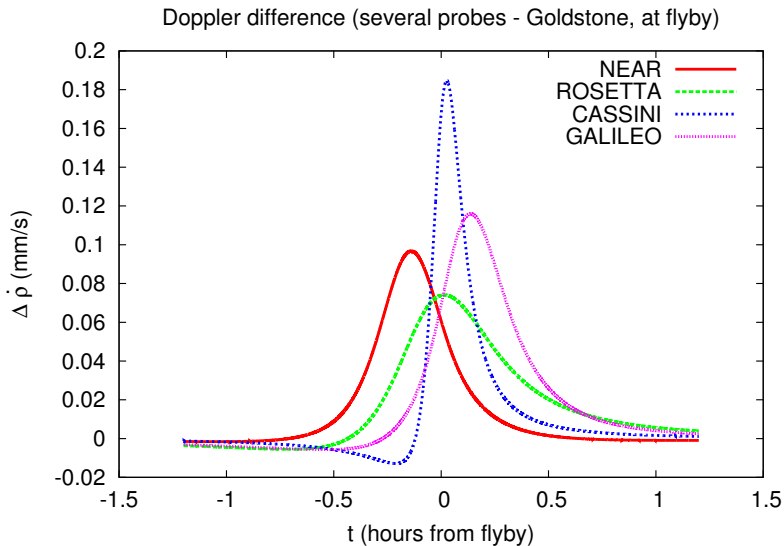


Figure 3: Doppler difference $\Delta\dot{\rho}$ (mm/s - hours from Earth flyby) for several probes with respect to Goldstone DSN station. The results highlight the high variability of the effect on Doppler measurements.

field. We first use the standard modeling for light time and Doppler and then compute alternative orbits by adding an arbitrary transponder delay of $2.5 \mu\text{s}$ to the light-time computations. The resulting orbit differences for the two satellites are shown in Table 2 and are well within the uncertainty value of the orbit recovery (estimated in several cm in radial direction and ≈ 1 m in the other directions).

Based on both orbit pairs, we then compute the Ka-band inter-satellite Range-Rate (KBRR), *i.e.* the radial velocity along the line-of-sight between the two satellites. Their difference shows a once-per-revolution signal with an amplitude of $\approx 0.1 - 1 \mu\text{m/s}$ in the along-track direction due to the mismodeling of the transponder delay. For completeness and to evaluate the impact of the transponder delay on the operative orbit recovery of the GRAIL probes, we perform a further orbit improvement by fitting both pair of orbits to Doppler and KBRR data. The relative weighting of these observables is usually chosen to strongly favor KBRR data (here we apply a $1 : 10^8$ ratio) because of their higher accuracy. A comparison of the resulting orbits then shows that post-fit KBRR differences due to the transponder delay are reduced to $\approx 0.001 \mu\text{m/s}$ (to be compared with the nominal KBRR accuracy

DOY	GRAIL	Radial	Along-Track	Cross-Track
12-063	A	0.08	0.62	2.96
	B	0.11	1.43	1.12
12-064	A	0.10	1.79	7.29
	B	0.10	0.67	2.72
12-072	A	0.08	1.11	0.10
	B	0.18	0.60	0.14
12-073	A	0.04	0.16	0.45
	B	0.04	1.01	0.87

Table 2: Orbit differences (mm, orbit frame) caused by introducing the transponder delay in the Doppler modeling for the orbit improvement process. During Day of Year (DOY) 12-063/064 the orbital plane of the GRAIL satellites is parallel to the line of sight w.r.t. Earth, while it is perpendicular for DOY 12-072/073.

of $0.03 \mu\text{m/s}$). KBRR residuals result globally improved by our updated light-time algorithm, but well below the formal uncertainties.

5.3. Application to ESA BepiColombo mission

We use the BSW to simulate two-way X-band Doppler for BepiColombo Mercury Planetary Orbiter (MPO) nominal orbit retrieved from ESA Spice SPK for 08/04/2025. We first compute Doppler data as observed by the Deep Space Network antennas following the standard formulation by Moyer (2003). Then, we include the transponder delay in the light-time modeling used for the simulation. We compute the resulting Doppler signal for several values of δt_{23} in the range $10^{-6} - 10^{-3}$ s and show the differences w.r.t. the standard formulation in Fig. 4. As shown in Table 1, MPO transponder delay has been measured at $4.8 - 6 \mu\text{s}$.

Our results highlight an additional frequency signal superposed to the orbital period and showing an amplitude linearly dependent from δt_{23} , as expected from Eq. (10). The amplitude of the additional signal, neglected in the standard formulation, is up to several mHz for slow transponders ($\delta t \approx 1$ ms) while it accounts for ≈ 0.02 mHz for modern transponders ($\delta t \approx 2.5 \mu\text{s}$). These values should be compared to the nominal accuracy of the MORE instrument (Iess and Boscagli, 2001), which is ≈ 5 mHz and ≈ 1.5 mHz at 10 seconds integration time for X- and Ka-bands, respectively (Cicalò et al., 2016). The impact of the transponder delay looks then safely below the noise level for the BepiColombo mission in its science phase.

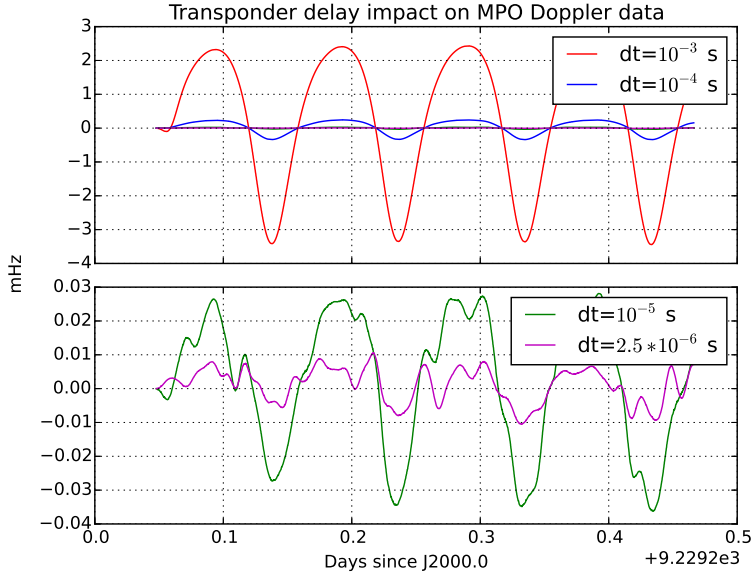


Figure 4: Doppler difference $\Delta\dot{\rho}$ for the nominal MPO orbit around Mercury on 08/04/2025 for different values of the transponder delay δt (1 mHz \approx 0.035 mm/s @ 8.4 GHz).

6. Conclusions

In this communication, we present a refinement of the formulation of two-way light-time for the tracking of space probes. In particular, we focus on the transponder delay, a tiny delay (amounting to several μs in modern devices) between the reception of the signal on the spacecraft and its re-emission towards Earth. It seems obvious from our results that the influence of the transponder delay cannot be reduced to a simple correction with a constant bias without taking some precautions. It is indeed responsible for a tiny effect on the computation of light time and has an impact on both range and Doppler determination. We take it into account by a more complete modeling, considering four events in the observables modeling instead of three as in Moyer.

In order to test the amplitude and variability of this effect on real data, we compute its influence on some real probe-ground station configurations during recent Earth flybys (NEAR, Rosetta, Cassini and Galileo). The observables calculated using the standard model and our updated one show differences of the order of several cm and of 0.1 mm/s for the range and the

range-rate, respectively. As expected from our analytical results, the impact of the transponder delay is maximized during a flyby maneuver, when the relative velocity between spacecraft and observer changes rapidly. Nevertheless, as already shown in Bertone et al. (2013), this effect can only account for a tiny portion of the so-called flyby anomaly. Moreover, we use the planetary extension of the Bernese GNSS Software to simulate the impact of several amplitudes of the transponder delay on both Doppler data and orbit recovery for the NASA GRAIL and ESA BepiColombo missions. To do so, we modify the light-time computation algorithm for the up-leg by requesting the probe ephemeris at an epoch anticipated of δt_{23} . The highlighted differences are acceptable for most operational goals at present, although applying a more accurate modeling could avoid the possible propagation of orbital errors in, *e.g.* the recovery of geophysical signatures or the analysis of tiny relativistic signals (Matousek, 2007) which could correlate with the effects of the transponder delay. Also, since the MORE instrument on-board BepiColombo will be equipped with an internal calibration circuit, it will be possible to measure the transponder delay and to systematically apply the updated formulation provided in this paper to test the impact on the data processing.

Finally, we stress that this error is directly proportional to the transponder delay. This means that this effect might be relevant for past missions equipped with slower transponders (whose data are still largely used for scientific purposes) or for long lasting missions when considering the degraded performances of aging transponders. In the future too, increasing spacecraft tracking accuracy (Iess et al., 2014) should be accompanied by the development of faster transponders or by correctly measuring, distributing and accounting for this delay in the orbit determination process.

7. Acknowledgments

SB acknowledges the financial support of the Swiss National Science Foundation (SNF) via the NCCR PlanetS. SB also thanks Dr. A. Hees for the helpful discussions. The authors thank G. Canepa and A. Busso of Thales Alenia Space for providing information about the transponder delay of several probes.

References

- Acton, C., Bachman, N., Diaz Del Rio, J., Semenov, B., Wright, E., Yamamoto, Y., 2011. SPICE: A Means for Determining Observation Geometry, in: EPSC-DPS Joint Meeting 2011, p. 32.
- Anderson, J.D., Campbell, J.K., Ekelund, J.E., Ellis, J., Jordan, J.F., 2008. Anomalous orbital-energy changes observed during spacecraft flybys of earth. *Physical Review Letters* 100, 091102. doi:[10.1103/PhysRevLett.100.091102](https://doi.org/10.1103/PhysRevLett.100.091102).
- Bertone, S., Jggi, A., Arnold, D., Beutler, G., L., M., 2015. Doppler Orbit Determination of Deep Space Probes by the Bernese GNSS Software: First Results of the Combined Orbit Determination from DSN and Inter-Satellite Ka-Band Data from the Grail Mission, in: 25th International Symposium on Space Flight Dynamics ISSFD. URL: http://issfd.org/2015/files/downloads/papers/174_Bertone.pdf.
- Bertone, S., Le Poncin-Lafitte, C., Lainey, V., Angonin, M.C., 2013. Transponder delay effect in light time calculations for deep space navigation. ArXiv e-prints [arXiv:1305.1950](https://arxiv.org/abs/1305.1950).
- Bertone, S., Minazzoli, O., Crosta, M., Le Poncin-Lafitte, C., Vecchiato, A., Angonin, M.C., 2014. Time transfer functions as a way to validate light propagation solutions for space astrometry. *Classical and Quantum Gravity* 31, 015021. doi:[10.1088/0264-9381/31/1/015021](https://doi.org/10.1088/0264-9381/31/1/015021), [arXiv:1306.2367](https://arxiv.org/abs/1306.2367).
- Busso (TAS-I), A., 2010. private communication.
- Cicalò, S., Schettino, G., Di Ruzza, S., Alessi, E.M., Tommei, G., Milani, A., 2016. The BepiColombo MORE gravimetry and rotation experiments with the ORBIT14 software. *MNRAS* 457, 1507–1521. doi:[10.1093/mnras/stw052](https://doi.org/10.1093/mnras/stw052).
- Dach, R., Lutz, S., Walser, P., Fridez, P. (Eds.), 2015. Bernese GNSS Software - Version 5.2. Astronomical Institute, University of Bern.
- Degnan, J., 2002. Asynchronous laser transponders for precise interplanetary ranging and time transfer. *Journal of Geodynamics* 34, 551–594. doi:[10.1016/S0264-3707\(02\)00044-3](https://doi.org/10.1016/S0264-3707(02)00044-3).

- Fienga, A., Laskar, J., Morley, T., Manche, H., Kuchynka, P., Le Poncin-Lafitte, C., Budnik, F., Gastineau, M., Somenzi, L., 2009. Inpop08, a 4-d planetary ephemeris: from asteroid and time-scale computations to esa mars express and venus express contributions. *Astronomy and Astrophysics* 507, 1675–1686. doi:[10.1051/0004-6361/200911755](https://doi.org/10.1051/0004-6361/200911755), [arXiv:0906.2860](https://arxiv.org/abs/0906.2860).
- Folkner, W.M., Williams, J.G., Boggs, D.H., Park, R.S., Kuchynka, P., 2014. The Planetary and Lunar Ephemerides DE430 and DE431. *Interplanetary Network Progress Report* 196, 1–81.
- Galanti, E., Durante, D., Finocchiaro, S., Iess, L., Kaspi, Y., 2017. Estimating Jupiter’s Gravity Field Using Juno Measurements, Trajectory Estimation Analysis, and a Flow Model Optimization. *AJ* 154, 2. doi:[10.3847/1538-3881/aa72db](https://doi.org/10.3847/1538-3881/aa72db).
- Genova, A., Marabucci, M., Iess, L., 2012. Mercury radio science experiment of the mission bepicolombo. *Memorie della Societ Astronomica Italiana* 20.
- Hees, A., Bertone, S., Le Poncin-Lafitte, C., 2014a. Light propagation in the field of a moving axisymmetric body: Theory and applications to the Juno mission. *Phys. Rev. D* 90, 084020. doi:[10.1103/PhysRevD.90.084020](https://doi.org/10.1103/PhysRevD.90.084020), [arXiv:1406.6600](https://arxiv.org/abs/1406.6600).
- Hees, A., Bertone, S., Le Poncin-Lafitte, C., 2014b. Relativistic formulation of coordinate light time, Doppler, and astrometric observables up to the second post-Minkowskian order. *Phys. Rev. D* 89, 064045. doi:[10.1103/PhysRevD.89.064045](https://doi.org/10.1103/PhysRevD.89.064045), [arXiv:1401.7622](https://arxiv.org/abs/1401.7622).
- Hees, A., Folkner, W.M., Jacobson, R.A., Park, R.S., 2014c. Constraints on modified Newtonian dynamics theories from radio tracking data of the Cassini spacecraft. *Phys. Rev. D* 89, 102002. doi:[10.1103/PhysRevD.89.102002](https://doi.org/10.1103/PhysRevD.89.102002), [arXiv:1402.6950](https://arxiv.org/abs/1402.6950).
- Iess, L., Boscagli, G., 2001. Advanced radio science instrumentation for the mission BepiColombo to Mercury. *Planet. Space Sci.* 49, 1597–1608. doi:[10.1016/S0032-0633\(01\)00096-4](https://doi.org/10.1016/S0032-0633(01)00096-4).

- Iess, L., Di Benedetto, M., James, N., Mercolino, M., Simone, L., Tortora, P., 2014. Astra: Interdisciplinary study on enhancement of the end-to-end accuracy for spacecraft tracking techniques. *Acta Astronautica* 94, 699–707. doi:[10.1016/j.actaastro.2013.06.011](https://doi.org/10.1016/j.actaastro.2013.06.011).
- Konopliv, A.S., Borderies, N.J., Chodas, P.W., Christensen, E.J., Sjogren, W.L., Williams, B.G., Balmino, G., Barriot, J.P., 1993. Venus gravity and topography: 60th degree and order model. *Geophysical Research Letters* 20, 2403–2406. doi:[10.1029/93GL01890](https://doi.org/10.1029/93GL01890).
- Lemoine, F.G., Goossens, S., Sabaka, T.J., Nicholas, J.B., Mazarico, E., Rowlands, D.D., Loomis, B.D., Chinn, D.S., Neumann, G.A., Smith, D.E., Zuber, M.T., 2014. GRGM900C: A degree 900 lunar gravity model from GRAIL primary and extended mission data. *Geophys. Res. Lett.* 41, 3382–3389. doi:[10.1002/2014GL060027](https://doi.org/10.1002/2014GL060027).
- Linet, B., Teyssandier, P., 2013. New method for determining the light travel time in static, spherically symmetric spacetimes. Calculation of the terms of order G^3 . *Classical and Quantum Gravity* 30, 175008. doi:[10.1088/0264-9381/30/17/175008](https://doi.org/10.1088/0264-9381/30/17/175008), [arXiv:1304.3683](https://arxiv.org/abs/1304.3683).
- Matousek, S., 2007. The Juno New Frontiers mission. *Acta Astronautica* 61, 932–939. doi:[10.1016/j.actaastro.2006.12.013](https://doi.org/10.1016/j.actaastro.2006.12.013).
- Milani, A., Rossi, A., Vokrouhlický, D., Villani, D., Bonanno, C., 2001. Gravity field and rotation state of Mercury from the BepiColombo Radio Science Experiments. *Planet. Space Sci.* 49, 1579–1596. doi:[10.1016/S0032-0633\(01\)00095-2](https://doi.org/10.1016/S0032-0633(01)00095-2).
- Montenbruck, O., Gill, E., 2000. *Satellite Orbits*. Springer-Verlag Berlin Heidelberg.
- Moyer, 2003. *Formulation for Observed and Computed Values of Deep Space Network Observables*. Hoboken, NJ.
- Petit, G., Luzum, B.e., 2010. IERS Conventions (2010). IERS Technical Note 36, 1.
- Shapiro, I.I., 1964. Fourth test of general relativity. *Physical Review Letters* 13, 789–791. doi:[10.1103/PhysRevLett.13.789](https://doi.org/10.1103/PhysRevLett.13.789).

- Srinivasan, D.K., Perry, M.E., Fielhauer, K.B., Smith, D.E., Zuber, M.T., 2007. The Radio Frequency Subsystem and Radio Science on the MESSENGER Mission. *Space Sci. Rev.* 131, 557–571. doi:[10.1007/s11214-007-9270-7](https://doi.org/10.1007/s11214-007-9270-7).
- Teyssandier, P., Le Poncin-Lafitte, C., 2008. General post-minkowskian expansion of time transfer functions. *Classical and Quantum Gravity* 25, 145020. doi:[10.1088/0264-9381/25/14/145020](https://doi.org/10.1088/0264-9381/25/14/145020), [arXiv:0803.0277](https://arxiv.org/abs/0803.0277).
- Zuber, M.T., Smith, D.E., Watkins, M.M., Asmar, S.W., Konopliv, A.S., Lemoine, F.G., Melosh, H.J., Neumann, G.A., Phillips, R.J., Solomon, S.C., Wieczorek, M.A., Williams, J.G., Goossens, S.J., Kruizinga, G., Mazarico, E., Park, R.S., Yuan, D.N., 2013. Gravity Field of the Moon from the Gravity Recovery and Interior Laboratory (GRAIL) Mission. *Science* 339, 668–671. doi:[10.1126/science.1231507](https://doi.org/10.1126/science.1231507).